

TURBULENCE AND SEDIMENT TRANSPORT MEASUREMENTS WITH A NEW TWO COMPONENTS ULTRASONIC PROFILER

GUTA H. ⁽¹⁾, FISCHER S. ⁽²⁾, DUFOUR D. ⁽²⁾, BURCKBUCHLER M. ⁽²⁾ & FROMANT G. ⁽¹⁾

⁽¹⁾ *Laboratory of Geophysical and Industrial Flows, Grenoble, France*

⁽²⁾ *UBERTONE, Strasbourg, France, info@ubertone.fr*

ABSTRACT

In the present paper, new data set of co-located 2C velocity and sediment concentration time-resolved measurements under steady uniform turbulent rough clear water and sheet-flow, performed with an Acoustic Concentration and Velocity Profiler (ACVP) and a prototype for a commercial ADV, the UB-MES, are presented. The flow regime for the measurement with both devices was similar. Comparisons of mean profiles of fluid velocity, Reynolds shear stress and turbulence intensities showed good agreements, with a mean relative error below 10% in clear water flow conditions. Time-resolved turbulence measurements also displayed a good agreement between the systems. The quadrant threshold distribution showed that both ejections and sweeps are the dominant turbulent bursting events in clear water uniform rough flow. Good agreement was also observed in sheet-flow measurements from ACVP and UB-MES. Comparisons of mean velocity profiles, sediment concentration and sediment flux under sheet-flow, revealed relative differences below 20%. The quadrant analysis showed different dynamics from clear water flow. Sweeps seem to be the dominant events particularly in the near-bed region, followed by outward interactions. However, in the upper region of the flow, ejections and sweeps become the two dominant turbulent bursting events, as in clear water flow. The conformity with results from previous studies performed in similar flows conditions supports the good performance of the UB-MES for turbulence measurements and sediment flux profiling.

Keywords: ACVP, multi-component velocity, sheet-flow, turbulent flow, sediment transport.

1. INTRODUCTION

Sediment transport prediction or modelling in intense flow regimes is crucial to a wide range of problematics (eg. river morphology, coastal bathymetry, evolution of shorelines (coastal) and lateral banks (rivers), risks of scouring of bridges, siltation of reservoir upstream of a dam wall.... Sediment transport occurs indeed during extreme events such as floods in rivers, or storms in coastal areas, and impacts the long-term morphological evolution. During events of extreme intensity, the bedload moves as a sheet-flow, a regime characterized by the occurrence of a dense layer of particles over the sediment bed. Under such conditions, both the granular interactions and turbulent processes are the key mechanisms in the momentum diffusion (Revil-Baudard et al. 2016) driving the transport.

As the dimension of sediments is relatively small compared to the one of the flow, turbulence plays an essential role in all flows of a water-sediment mixture (Graf & Altinakar 1998). Thus, turbulence measurements in clear water flow provide useful information concerning sediment-laden hydrodynamic processes. General consensus has been reached regarding several issues concerning the turbulent flow properties in clear water, but the understanding of turbulence modifications and impact on sediment transport still faces many challenges, especially in the bottom boundary layer of the flow. An example is our limited understanding of particle diffusion process, greatly influenced by turbulence effects on settling velocity.

In order to improve our understanding of the physical processes involved in sediment transport, and thus improve our capability to model this transport, the need of high resolution measurements is evident. However, our ability to profile within the bottom boundary layer is limited to a few measurement technologies, such as gamma-ray and conductivity techniques in pipe flows (Wilson 1966, Nnadi & Wilson 1992, Pugh & Wilson 1999), capacitance probes (Summer et al. 1996), boroscopic probes, video technique (Armanini et al. 2005, Spinewine et al. 2011; Capart & Fraccarollo 2011) for instantaneous 2C particle velocity and mean concentration profiles. In the past years, an Acoustic Concentration and Velocity Profiler (Hurther et al. 2011) has been developed, and revealed new insights concerning the hydrodynamic processes in the near-wall region. A prototype for a commercial version of the ACVP has been developed by French company UBERTONE, the UB-MES. Here, a new set of high-resolution measurements of co-located 2-Components (2C) velocities and sediment concentration profiles collected with a UB-MES prototype and an ACVP in an experimental tilting flume, under clear water and sheet-flow condition is presented.

The aim of the study is to evaluate the performances of the UB-MES in terms of mean flow properties and time-resolved turbulence measurements in clear water flow, as well as sediment flux profiling in sheet-flows. Additionally, a brief analysis of turbulent bursting events in clear water and sheet-flow based on quadrant distribution is performed.

The structure of the paper is as follows: in section 2 the experimental setup and flow conditions are presented. The mean flow properties and time-resolved turbulence measurement results in clear water are presented and discussed in section 3. In section 4, the sheet flow results are presented. The mean sediment flux measurement capabilities of UB-MES are finally discussed in section 5.

2. METHODOLOGY

2.1 Experimental setup and instrumentation

The experiments were carried out at the LEGI, using a 10 m long tilting flume, with 0.35 m width. Different slopes were set for clear water experiments and for sheet-flow experiments. For sheet flow experiments, the (rectangular) sediment pit, located at 5 m from the beginning of the channel is $3 \times 0.11 \text{ m}^2$, is initially filled with low density ($\rho_p=1192 \text{ kg/m}^3$) non-spherical plastic sediments (Poly-Methyl MethAcrylate) of median diameter $d_p=3 \text{ mm}$ and the packed volumetric concentration is 0.55. The settling velocity w_s of the particles is 5.6 cm/s. The fixed bed is covered by glued particles, with the same properties as the sediments filled in the channel. For the clear water measurements, the fixed bed is placed in the sediment pit. For both conditions (clear water and sheet flow), a sluice gate at the downstream end and a by-pass at the upstream end allow to regulate the flow discharge as shown in Figure 1.

The velocity profiling principle of these acoustic systems is based on the Acoustic Doppler Velocity Profiler technology. The ACVP has one emitter and two (convergent) receivers. Employing the two receivers allows the measurement of two Doppler frequencies at the same time and point along the common emitter axis. The streamwise velocity and the flow normal velocity are then obtained from the Doppler shift frequencies. Same sensors (emitter and receivers) were used with ACVP and UB-MES in order to compare exclusively the functioning of the systems. The volumetric concentration is retrieved by inversion of the output of the mean squared voltage signal. This inversion requires the knowledge of the backscattering properties of the particles, water absorption along the profile, the system depending parameters and the attenuation coefficient, as detailed in Hurther et al. 2011. For both acoustic systems, the carrier frequency was set to 1 MHz, with a pulse duration of $2 \mu\text{s}$ allowing a vertical spatial resolution of 1.5 mm. The obtained time resolutions were 19 Hz for velocity and 4.8 Hz for concentration, for sheet-flow measurements.

2.2 Experimental protocol and flow properties

The sheet-flow experimental protocol from (Revil-Baudard et. al, 2015) was applied. The experiments are performed with no recirculation of the sediments. In such conditions, after a short period at the beginning of the experiment, the sediments placed in the pit are eroded (see figure 1). Each experiment lasted less than two minutes. Thus for proper statistical convergence of the flow quantities, the experimental runs were repeated several times. Figure 2 displays the time evolution of the bed interface for ACVP (2a) and UB-MES (2b). An initial transient phase can be observed with both systems, in which the bed erosion rate reaches its peak value, followed by a quasi-uniform phase of the flow, with a fairly steady bed erosion rate, which lasts about 30 s.

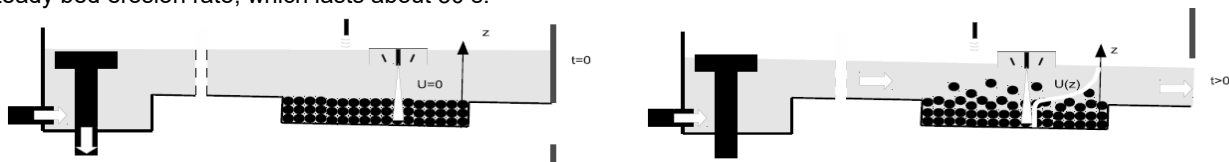


Figure 1. Sketch of experimental set up in its initial ($t=0$) and running ($t>0$) states

For clear water experiments, no particular protocol was implemented since the sediment pit was covered by fixed rough bed plates. It was only necessary to approach the uniform flow conditions for which the mean flow and turbulence properties are well known and described in the literature (Nezu and Nakagawa 1993).

For both clear water and sheet-flow conditions, the flow was highly turbulent, hydraulically rough and subcritical (Table 1), as indicated by the high Reynolds number ($Re = UH_f/\nu > 2000$), the high bed roughness Reynolds number ($Re^* = u_{*} ks/\nu > 70$) and the low Froude number ($Fr = U/\sqrt{gH_f} < 1$).

Table 1. Sediment and flow properties in Clear water (CW) and Sheet-flow (SF)

	S_0 (%)	d_p (mm)	N (-)	w_s (cm/s)	u_* (cm/s)	ρ_p (kg/m ³)	H_f (m)	Q (m ³ /s)	U (m/s)	Re	Re*	Fr
CW _(ACVP & UB-MES)	0.375	-	-	-	5.7	-	0.12	28,9	0.69	8×10^4	428	0.6
SF _(ACVP)	0.5	3.0	4	5.6	4.3	1192	0.135	28.8	0.59	8×10^4	304	0.5
SF _(UB-MES)	0.5	3.0	5	5.6	4.1	1192	0.145	28.8	0.55	8×10^4	322	0.5

S_0 : Slope of the channel; U : bulk mean velocity; H_f : water depth; ν : kinematic viscosity of water; u_* : friction velocity; ks : equivalent roughness ($ks=2.5 d_p$ for mobile bed experiments and $ks=3 \text{ mm}$ for clear water) and g is the gravitational acceleration

2.3 Validation and Calibration of UB-MES measurements

The ability of the ACVP for high resolution measurements of velocity, concentration and sediment flux profiles has been showed by several authors (Hurther et al. 2011, Hurther and Thorne 2011, Naqshband et al. 2014, Revil-Baudard et al 2015,2016, Fromant et al. 2018). The mean sediment flux is estimated over the quasi-steady time interval $T=t_2-t_1$.

$$q_s = \frac{1}{T} \int_{t_1}^{t_2} \int_{z_b}^{H_f} u(z,t)C(z,t) dz dt \quad (2.4)$$

where $u(z,t)$ and $C(z,t)$ are respectively the instantaneous streamwise velocity and volumetric concentration, z_b is the bed interface level and H_f is the water flow depth. In the present study, the sediment flux profiling was performed under similar flow conditions as in Fromant et al. 2018, for which ACVP measurements have been validated. The same set of transducers was used with both ACVP and UB-MES systems. However, because of the different internal electronic characteristics, a calibration ratio between the echo intensities recorded by both systems was determined in order to apply the same acoustic inversion methodology as described in Fromant et al. 2018.

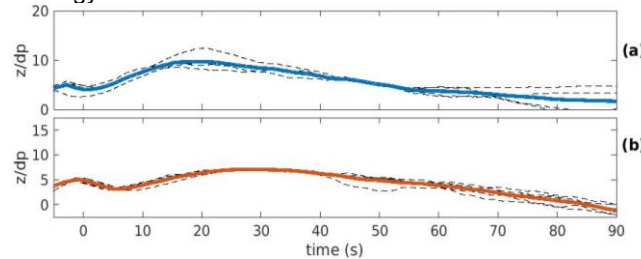


Figure 2. Time evolution of the bed interface position filtered at 0.1 Hz and made dimensionless by the particle diameter for individual runs (dashed lines); ensemble average (solid lines); (a) ACVP; (b) UB-MES

2.4 Sheet flow Data processing methods

Figure 3a shows the accumulated volumes of transported sediments for all ACVP experiments and 3b for UB-MES. The order of magnitude of the total transported volumes from both systems is similar to Fromant et al. 2018, around 0.040 m^3 , which suggests that despite slight differences observed in flow conditions, the dynamics of the sediment transport was similar in these experiments. Based on the similar bed morphological evolution (Figure 2) and amount of transported sediment between runs, 4 experiments were selected from ACVP and 5 from UB-MES. Figures 3c and 3d display the accumulated volumes of transported sediments for the selected runs from ACVP and UB-MES, respectively. Due to bed erosion (and the absence of a sediment collection and recirculation system), the position of the bed interface evolves with time. In order to average the flow properties over the entire quasi-steady phase of about 30 s, bed referencing was applied. This consisted in adjusting the bed interface position based on a reference position all along the duration of the run, thus defining a time-varying origin at the bed position. This procedure has been applied to each run before ensemble averaging the bed referenced quantities (velocity, concentration) over the number of repeated runs.

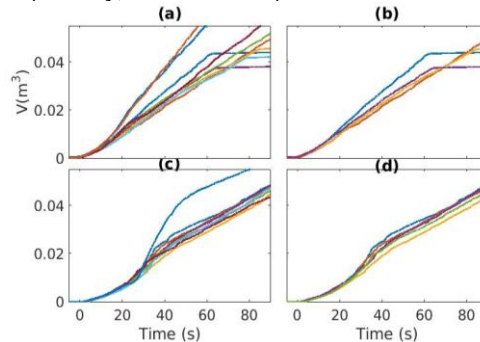


Figure 3. Accumulated volume of transported sediments for all the experiments with ACVP (a) and UB-MES (c). Accumulated volume of transported sediments for the selected experiments with ACVP (b) and UB-MES (d).

Following the same procedure and assumptions as in Revil-Baudard et al. 2015, the statistical properties of the ensemble averaged velocity, concentration and sediment flux over a time window of 30 s was defined as follows:

$$\langle A \rangle (z) = \frac{1}{N} \sum_{i=1}^N \left(\frac{1}{\Delta t} \int_{t_1}^{t_2} A_i(z,t) dt \right) \quad (2.8)$$

where $\Delta t=t_2-t_1=30 \text{ s}$, the operator $\langle - \rangle$ refers to an ensemble average (over N, the number of repeated experiments) of the temporal mean of quantity A.

3. RESULTS AND DISCUSSION – CLEAR WATER (CW)

In order to ensure the proper functioning of the UB-MES prototype, the first part of the analysis determines the fluid velocity measurement performances in terms of mean quantities: velocity profile, turbulence intensity profiles, shear

stress profiles and turbulent spectra. The quantification of the differences between the two systems will be described by the relative error μ , averaged over the points of the mean profiles and its standard deviation σ .

3.1 Mean velocity profile

Figure 4 (top) presents the vertical longitudinal mean velocity profiles measured by the ACVP and the UB-MES as functions of the bottom distance normalized by the water flow depth H_f . The agreement between the two measurements for $0 < z/H_f < 0.70$ is good. In the region $z/H_f > 0.70$, the flow is strongly disturbed by the presence of the box holding the sensors positioned at the free-surface height.

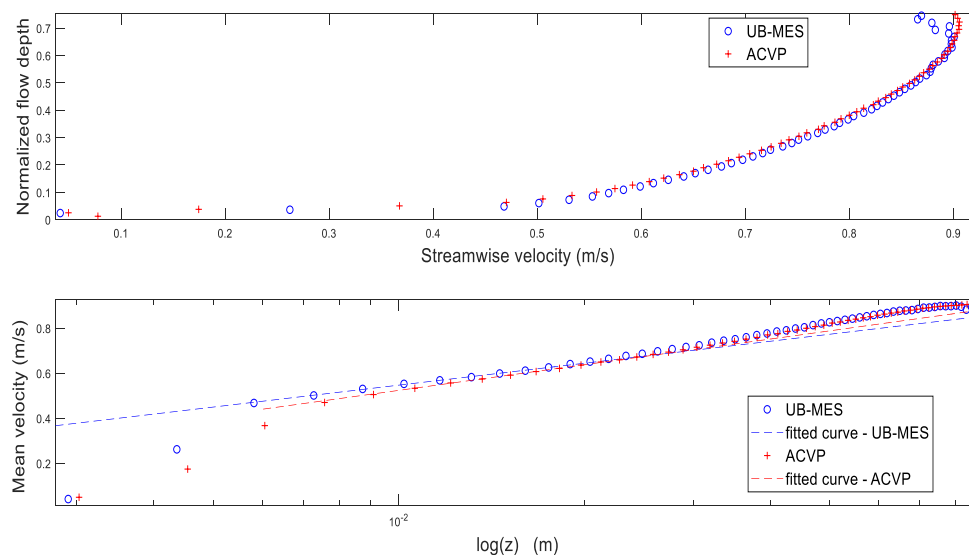


Figure 4. (top) Mean longitudinal velocity profiles for CW experiment; (bottom) mean velocity profiles in semi-logarithmic representation. ACVP (+, red) and UB-MES (o, blue). logarithmic fit for ACVP (---, red) and UB-MES (---, blue)

Figure 4 (bottom) shows the profiles on a semi-logarithmic scale to verify the validity of the logarithmic velocity profile based on the existence of the law of the wall and the concept of turbulent mixing length according to Prandtl (1926). The law of the wall, which allows the prediction of the velocity profile, can be written as follows:

$$u = \frac{u_*}{\kappa} \ln \left(\frac{z}{z_0} \right) \quad (3.1)$$

where u_* is the friction velocity (cm/s), κ is the von Karman parameter, with a value $\kappa=0.41$ in clear water and z_0 corresponds to the zero velocity level. The mean relative difference between the two systems is $\mu = 1.42\%$, with a standard deviation $\sigma = 0.44\%$, confirming the correct operation of the UB-MES for the mean velocity profile. From the value of the slope of the mean velocity profile adjusted to a logarithmic profile (dashed lines in figure 4 bottom) the two estimates of the bed friction velocity u_* are extracted. The values of $u_* = 5.8$ cm/s and $u_* = 6$ cm/s are obtained with the UB-MES and the ACVP respectively, confirming the agreement of the slopes of the profiles in the logarithmic zone.

3.2 Mean velocity profile

Figure 5 shows the turbulence intensity profiles for the horizontal and vertical velocity components as a function of the (normalized by the friction velocity) distance to the wall. The agreement between UB-MES and ACVP measurements over the entire vertical profile is good. The differences observed for $z/H_f < 0.1$ can be attributed to the presence of the roughness sublayer (as mentioned above) in which a spatial variation of the time-averaged hydrodynamic quantities is seen at the scale of the glued particles size $d_p = 3$ mm. Differences of positioning between the ACVP and UB-MES data can be explained by the placement of the sensor structure, which is not repeatable on the millimeter scale. The measurements of turbulence intensities obtained by the two instruments reveal the same degree of anisotropy between horizontal and vertical components, which is induced by the average friction exerted by the flow on the rigid rough bottom (sheared boundary layer on rough wall).

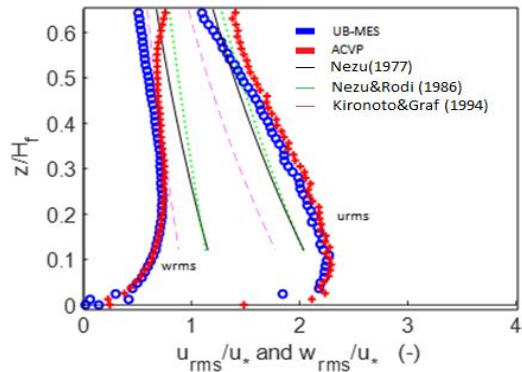


Figure 5. Normalized mean turbulence intensity profiles.

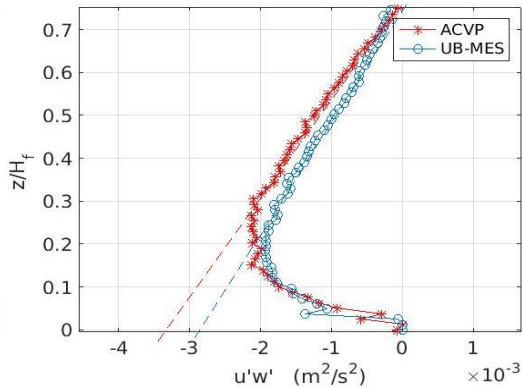


Figure 1. Mean Reynolds shear stress profiles

The values of the normalized intensities as well as the shapes of the associated profiles (figure 5) are close to those found in the literature for rough open channel turbulent flows (Nezu 1977, Nezu and Nakagawa 1993, Kironoto and Graf 1994). The agreements with the literature, as well as with ACVP, support the validity of the UB-MES measurement of turbulent intensities.

3.3 Mean turbulence intensity

Figure 6 compares the turbulent shear stress profiles versus the water level-normalized distance to the bottom. Both profiles have excellent linearity for $z / H_f > 0.25$, reflecting the uniformity of the studied free-surface flow. The (total) bed shear stress was estimated by the extrapolation of the Reynolds shear stress up to the wall. The mean relative differences and their standard deviations remain well below 10% but with ACVP values systematically higher than those estimated by the UB-MES (see table 2). The resulting difference between the two friction rates obtained by linear extrapolation of the two shear profiles at the bottom position is less than 10%. It should be noted that this higher value obtained with the ACVP remains consistent with the higher value obtained previously by logarithmic adjustment of the two mean velocity profiles (Figure 4), suggesting that the flow rate during the ACVP measurement was higher. Finally, it can be seen that the zero shear point (far from the wall) of the two linearly adjusted profiles does not operate at $z / H_f = 1$ but at a standardized distance of the bottom equal to 75%. This reflects the disturbance of free-surface flow due to sensor intrusion. The mean relative differences between the mean profiles are presented in table 2; they are all well (below 10%).

Table 2 Mean and standard deviations of relative differences between UB-MES and ACVP measurements.

	Experience CW							
	\bar{u}		u_{rms}/u_*		w_{rms}/u_*		$\overline{u'w'}$	
	μ (%)	σ (%)	μ (%)	σ (%)	μ (%)	σ (%)	μ (%)	σ (%)
UB-MES vs. ACVP	1.42	0.44	2.56	1.25	3.62	3.82	7.27	3.75

3.4 Turbulence spectra

To further validate turbulence intensity measurements of the UB-MES, the power spectral densities of the temporal velocity fluctuations are shown in Figures 7. As seen in the turbulent intensity profiles, the strong anisotropy between the spectra in u (longitudinal component) and w (vertical component) is observed at low frequency and decreases strongly at higher frequencies. Such behavior confirms a tendency of smaller isotropic turbulent structures, as suggested by the turbulent energy cascading theory of Kolmogorov (1941). For the 3 vertical positions, there is excellent agreement between the UB-MES and ACVP spectra for each of the components. On the other hand, the presence of a slope break of the spectra appearing at the same frequency values for the 2 measurement systems, as well as the $-5/3$ frequency tradeoff beyond this break (especially for the vertical component w) illustrates the identical operation of the two high-resolution measurement systems and the existence of turbulent kinetic energy cascade in the inertial zone based on the Kolmogorov theory (1941).

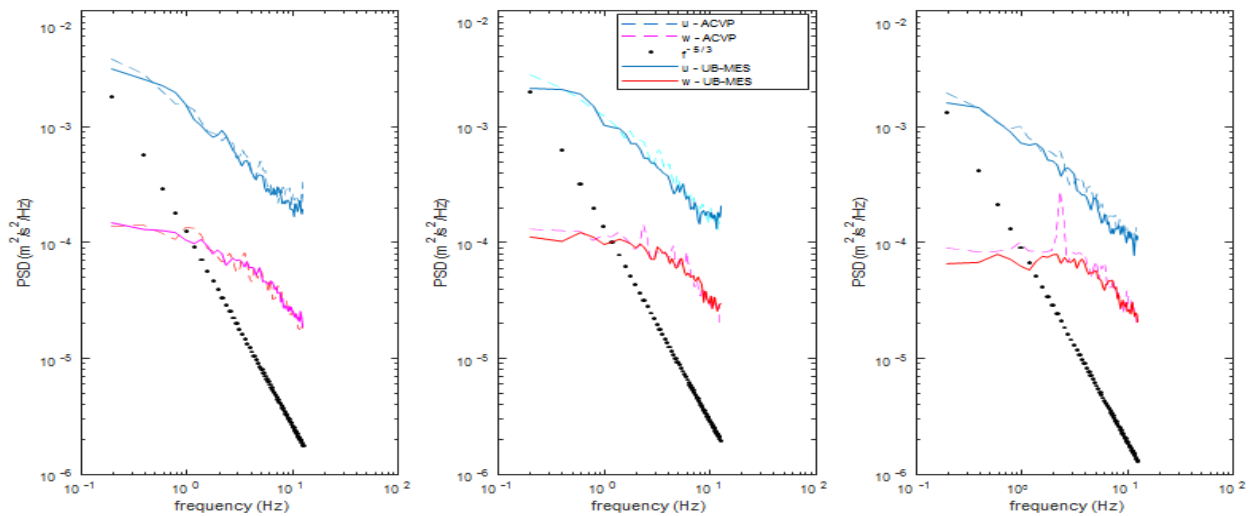


Figure 6. Turbulent spectra of the horizontal (blue) and vertical (red) components at $z/H_f=0.15$ (left), $z/H_f=0.30$ (center) and $z/H_f=0.45$ (right); Dotted spectra correspond to $f^{-5/3}$ spectra

3.5 Turbulent bursting events – Clear Water

Large scale turbulent structures and bursting events are relevant in understating sediment entrainment process in turbulent flows. Turbulent bursting events can be quantified from conditional statistics of velocity fluctuations u' and w' (Nezu and Nakagawa 1993, Hurther et al. 2007, Revil-Baudard et al. 2016).

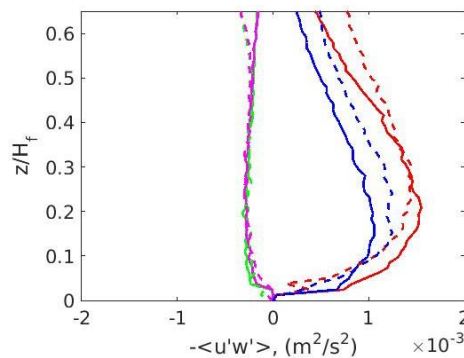


Figure 7. Quadrant threshold distribution for shear stress using $H=0$ for ACVP (dashed lines, a) and for UB-MES (solid lines, b). blue=sweeps, red=Ejections, green=Outward interactions and purple=Inward interactions.

This procedure allows to evaluate the total Reynolds shear stress at a given point as a sum of contributions from different bursting events, which are distinguished according to the quadrant in $u'w'$ plane (Lu & Willmarth 1973), and the respective threshold level H : outward interactions $Q = 1$ ($u' > 0, w' > 0$), ejections $Q = 2$ ($u' < 0, w' > 0$), inward interactions $Q = 3$ ($u' < 0, w' < 0$) and sweeps $Q = 4$ ($u' > 0, w' < 0$).

Figure 8 presents the quadrant threshold distribution, as described by Nezu and Nakagawa 1993, for the shear stress with $H=0$. Ejections and sweeps are the predominant events in the measurements from both systems, which is consistent with the literature (Nezu & Nakagawa 1993, Dey 2015, Revil-Baudard et al. 2016).

4. RESULTS AND DISCUSSION – SHEET-FLOW

By comparing mean velocity profiles, concentration and sediment flux measured by the ACVP and by UB-MES, the sediment flux profiling capability of UB-MES is analyzed in this section. The friction velocity u^* estimated from the extrapolated Reynolds shear stress, was about 4.1 cm/s for UB-MES and 4.3 cm/s for ACVP. The corresponding Shields number θ was about 0.3 for both systems, and it shows also a good agreement with respect to Fromant et al (2018), in which $u^*=4.1$ cm/s. The suspension number, $ws/u^*=1.4$ and 1.3 for UB-MES and ACVP respectively.

4.1 Mean profiles comparison

In figure 9 vertical profiles of streamwise velocity (a), volumetric particle concentration (b), and sediment flux repartition from ACVP (+) and UB-MES (o) are presented. The profiles were limited to the vertical range where most of the particle transport occurs. The vertical axis z was normalized by the particle diameter. The elevation $z=0$ corresponds to the bed interface.

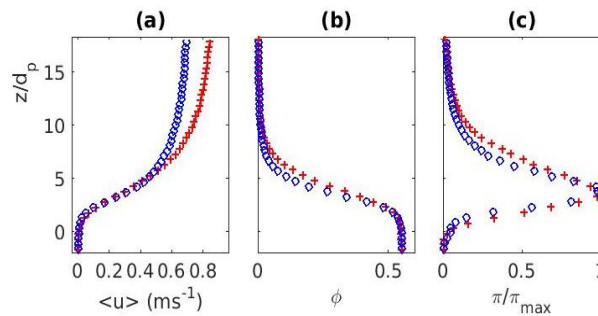


Figure 8. Mean profiles of streamwise velocity (a), volumetric concentration (b) and normalized sediment flux (c) for the ACVP (+) and UB-MES (o).

Figure 9a displays the mean streamwise velocity profiles for ACVP (+) and UB-MES (o). The relative difference between UB-MES and ACVP increased with elevation up to 14% at the top of the profiles. Such difference is attributed to different flow conditions, despite the same flow regime, as indicated by the same order of magnitude of the flow parameters (Table 1). Despite similarities with the clear water velocity distribution, the law of the wall cannot be directly applied in this flow conditions, as previously shown by Revil-Baudard et al. (2015). One reason is the reduction of the von Karman parameter (equal to $\kappa=0.41$ in clear water) in sediment-laden flows. Estimations of the von Karman parameter based on linear mixing length fitting $l_m(z) = k(z - z_D)$ resulted in approximately $\kappa=0.24$ with both systems.

Figure 9b shows that concentration decreased with increasing z , from its maximum value 0.55, with distinct trends along the flow depth. It decreased linearly for $2 < z/d_p < 4$ and then it decreased exponentially with z , as the well-known Rouse (1937) profile. The sheet layer thickness, which corresponds to the region of high volumetric concentration $0.08 < \phi < 0.55$ (Fromant et al. 2018), was also quantified. Both systems evaluated sheet layer thicknesses of approximately $5d_p$, which is consistent with Fromant et al (2018), who reported $\delta \sim 5 d_p$, and Revil-Baudard et al. 2015 data, from which $\delta \sim 5 - 6 d_p$ were estimated following the same methodology. This is an important indication not only of a good agreement between the two systems in the concentration profiling, but also with the previous measurements under similar flow conditions.

The vertical distribution of the sediment flux normalized by its maximum value is presented in figure 9c. The ACVP displays slightly wider flux profiles than the UB-MES. The mean sediment flux π (per meter width, over the quasi-steady interval) estimated with UB-MES and ACVP are respectively 7.5 and 9.3 m^2/s . The relative difference in mean sediment flux predicted by the UB-MES with respect to ACVP is below 20%, which strongly suggests the good capabilities of the UB-MES to measure sediment flux. The lower mean sediment flux observed in the UB-MES measurements with respect to ACVP is consistent with the observed differences in terms of velocities. This confirms that the flow was slightly more energetic during measurements with the ACVP.

4.2 Turbulent bursting events – Sheet-flow

Contrary to clear water flows, ejections (Q2) don't have an important contribution to the turbulent shear stress in the near-bed region. These results are similar to Revil-Baudard et al 2016, who argued that this may be attributed to an increase in roughness sublayer, when compared to clear water. The author also argues that this is true if the sublayer thickness is taken as the height at which ejections and sweeps contribution have the same order of magnitude. Additionally, the observed dominance of sweeps in the near-bed region was previously reported by Nezu and Nakagawa (1993) and Franca et al. (2014), in hydraulically rough flows.

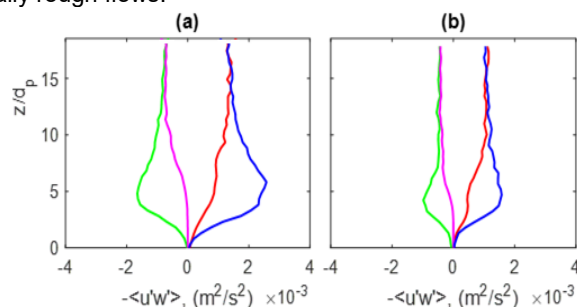


Figure 9. Quadrant threshold distribution for shear stress using $H=0$ for ACVP (a) and for UB-MES (b). blue=sweeps, red=Ejections, green=Outward interactions and purple=Inward interactions.

5. CONCLUSIONS AND PERSPECTIVES

In the present study, the UB-MES capabilities of turbulence measurements in clear water and high-resolution profiling of velocity, concentration and sediment flux under sheet-flow conditions were evaluated, using ACVP measurements as a reference. A good agreement was observed between the measurements from the two systems, as the relative differences are below 10% in clear water and 20% in sheet-flow. Regarding the sheet-flow conditions, differences in the flow conditions were observed between the two systems, explaining the greater relative differences compared with clear water conditions.

Results from previous studies performed under similar flow conditions (Revil-Baudard et al. 2015; Fromant et al. 2018) support the potential of the UB-MES in terms of sediment flux profiling. This potential is further confirmed by the good agreement of the mean flow quantities with the literature.

The quadrant threshold analysis confirmed the dominance of ejections and sweeps in clear water. In sheet-flow, sweeps have shown to be dominant in the near bed region, while ejections contributions become greater in the upper region of the flow. This behavior was observed in both systems, highlighting the UB-MES ability to characterize turbulent bursting events, which play an important role in sediment entrainment processes.

REFERENCES

- Armanini, A., Capart, H., Fraccarollo, L. & Larcher, M. (2005) Rheological stratification in experimental free-surface flows of granular-liquid mixtures. *J. of Fluid Mech.* 532, 269–319.
- Capart, H. & Fraccarollo, L. (2011) Transport layer structure in intense bed-load. *Geophysical Research Letters* 38 (20), n/a–n/a.
- Dey, S. (2015) Fluvial Hydrodynamics: Hydrodynamic and Sediment Transport Phenomena. *Springer Verlag Berlin Heidelberg*.
- Franca, M.J.; Santos, B.O.; Antico, F. and Ferreira, R.M.L. (2014) Quadrant Analysis of Shear Events in Open Channel Flows Over Mobile and Immobile Hydraulically Rough Beds. *ERCOTAC Bulletin 100, September 2014*, pp. 29-36.
- Fromant, G., Mieras, R.S., Revil-Baudard, T., Puleo, J. A., Hurther, D. & Chauchat, J. (2018) On bed load and suspended load measurement performances in sheet-flows using acoustic and conductivity profilers. Under review in *J. Geoph Res: Earth Surface*.
- Graf, W. H. & Altinakar, M. S. (1998). FLUVIAL HYDRAULICS: flow and transport processes in channels of simple geometry. Wiley, Chichester.
- Hurther, D., Lemmin, U. & terray, E. A. (2007) Turbulent transport in the outer region of rough-wall open-channel flows: the contribution of large coherent shear stress structures (LC3S). *J. Fluid Mech.* 574, 465–493.
- Hurther, D. & Thorne, P. D. (2011) Suspension and near-bed load sediment transport processes above a migrating, sand-rippled bed under shoaling waves. *J. Geophys. Res.: Oceans* 116, C07001.
- Hurther, D., Thorne, P. D., Bricault, M., Lemmin, U. & Barnoud, J.M. (2011) A multifrequency acoustic concentration and velocity profiler (ACVP) for boundary layer measurements of fine-scale flow and sediment transport processes. *Coastal Engineering*. 58, 594–605.
- Kironoto, B.A. & Graf, W.H. (1994) Turbulence characteristics in rough uniform open-channel flow. *Water Marit Energy Proc Inst Civ Eng (London)* 106, 333–344.
- Kolmogorov, A. N. (1941) Dissipation of energy in locally isotropic turbulence, *Doklady Akademii Nauk*, vol. 32, 1941, p. 16-18
- Lu, S. S. & Willmarth, W. W. (1973) Measurements of the structure of the Reynolds stress in a turbulent boundary layer. *J. Fluid Mech.* 60, 481-511.
- Naqshband, S., Ribberink, J. S., Hurther, D. & Hulscher, S.J.M.H. (2014) Bed load and suspended load contributions to migrating sand dunes in equilibrium. *Journal of Geophysical Research: Earth Surface* pp. n/a–n/a
- Nezu I (1977) Turbulent structure in open channel flow. *PhD thesis, Kyoto University, Kyoto*.
- Nezu, I. & Nakagawa, H. (1993) Turbulence in Open-channel Flows. IAHR.
- Nnadi, F. N. & Wilson, K. C. 1992 Motion of contact-load particles at high shear stress. *Journal of Hydraulic Engineering* 118 (12), 1670–1684.
- Prandtl, L. (1926) Bericht über neuere turbulenzforschung. *Hydraulische Probleme* pp. 1–13.
- Pugh, F. J. & Wilson, K. C. (1999) Velocity and concentration distributions in sheet flow above plane beds. *J. Hydraul Eng* 125 (2), 117–125.
- Revil-Baudard, T., Chauchat, J., Hurther, D. & Barraud, P. A. (2015) Investigation of sheetflow processes based on novel acoustic high-resolution velocity and concentration measurements. *J. Fluid Mech.* 767, 1–30.
- Revil-Baudard, T., Chauchat, J., Hurther, D. & Eiff, O. A. (2016) Turbulence modifications induced by the bed mobility in intense sediment-laden flows. *J. Fluid Mech.*, 808, 469 - 484.
- Rouse, H. (1937). Modern conceptions of the mechanics of turbulence. *Trans. Am. Soc. Civ. Eng.* 102, 463–505.
- Spinewine, B., Capart, H., Fraccarollo, L. & Larcher, M. (2011) Laser stripe measurements of near-wall solid fraction in channel flows of liquid-granular mixtures. *Experiments in Fluids* 50, 1507–1525.
- Thorne PD, Williams JJ, Heathershaw AD (1989) In situ acoustic measurements of marine gravel threshold and transport. *Sedimentology* 36(1):61–74.
- Wilson, Kenneth C. (1966) Bed-load transport at high shear stress. In Proc. A.S.C.E, vol. HY6. ASCE.